



# Simulation and experimental investigations on water-lubricated squeeze film damping stern bearing

Wu Ouyang<sup>1,2,3</sup> · Qilong Yan<sup>1</sup> · Junxin Kuang<sup>1</sup> · Yong Jin<sup>1,3</sup> · Weicai Peng<sup>4</sup>

Received: 1 May 2020 / Accepted: 15 December 2020 / Published online: 8 January 2021  
© The Brazilian Society of Mechanical Sciences and Engineering 2021

## Abstract

In order to solve the contradiction between high load-carrying capacity and low natural frequency in designing ship water-lubricated stern bearing, an idea of independent design of load carrying and vibration reduction functions was proposed, and the squeeze film damper technology was innovatively introduced into a conventional water-lubricated stern bearing (CWSB) to form a water-lubricated damping stern bearing (WDSB). Harmonic responses of two bearings were calculated, and a dynamic characteristic experiment was carried out. The results show that the maximum displacement response (MDR) decreases with the increase in oil film clearance. With the increase in inner flange height, MDR increases first and then decreases. MDR decreases first and then increases with the increase in distribution angle. As rotation rate speeds, the difference between two bearings' Root Mean Square (RMS) vibration amplitude remains unchanged. As load increases, relative reductions of two bearings' maximum amplitude and RMS decrease. Amid a load of 0.2 MPa and a rotational speed of 200r/min, compared with CWSB, the maximum amplitude of WDSB in the vertical direction is reduced by about 71.8%, and the relative reduction in RMS is about 47.8%, which verifies the damping effect of WDSB is remarkable.

**Keywords** Water-lubricated stern bearing · Integral squeeze film damper · Vibration reduction · Harmonic response · Dynamic characteristic

## 1 Introduction

Propulsion shafting is an important part of the ship power system for transmission of main engine power and ship navigation. Running quality of shafting plays a key role in reducing ship vibration and noise. Vibration and noise, as a culprit, limit ship survival, and combat capability [1].

Especially for underwater vehicles, vibration, and noise, control of shafting has long been a topical issue [2]. The Stern bearing, a key component of the propulsion shafting, is used to bear the weight of the propeller and propeller shaft. Compared with oil-lubrication, water-lubrication with the characteristics of resource-saving, environmental friendliness, and noise absorption is most famous for warship's stern bearing.

As the first link element that transmits the shafting vibration to the base or even the hull, the vibration damping capability of the water-lubricated stern bearing (WSB) plays an important role in controlling the shafting vibration [3]. WSB consists of two parts: the lining and the bushing, wherein the lining is made of soft polymer composite material with good wear resistance and impact resistance. The operating conditions of WSB are not decent. Firstly, the low viscosity of water well reduces the carrying capacity of bearing. Secondly, as the tonnage increases, the propeller's weight increases, and the propeller shaft undergoes significant bending and misaligned [4], resulting in a serious local load on WSB of the length-diameter ratio (1/3 to 1/4). Moreover, the rotational

---

Technical Editor: Thiago Ritto.

---

✉ Wu Ouyang  
ouyangw@whut.edu.cn

<sup>1</sup> School of Energy and Power Engineering, Wuhan University of Technology, Wuhan 430063, China

<sup>2</sup> Reliability Engineering Institute, National Engineering Research Center for Water Transport Safety, Wuhan 430063, China

<sup>3</sup> Key Laboratory of Marine Power Engineering and Technology, Ministry of Transport, Wuhan 430063, China

<sup>4</sup> National Key Laboratory on Ship Vibration & Noise, China Ship Development and Design Center, Wuhan 430064, China

speed is low, about 15 ~ 200 r/min, and it is often submerged at very low speed. In short, under the harsh conditions, the interface of WSB is in a mixed lubrication state [5], which is prone to local contact friction [6] and wear [7], causing abnormal noise [8], and shaft vibration [9].

Research on reducing vibration methods of bearing from various aspects has been carried out. In the improvement of lining material, two methods of adding reinforcing elements and stacked structure have appeared. Among them, rubber material modification is based on rubber as the matrix. By adding reinforcing elements [10] or superimposing reinforcing layers [11, 12], the advantages of rubber, such as high elasticity and vibration absorption, are retained, and the deficiencies of rubber, such as low limit carrying capacity and low-speed noise, are improved. After modifying, the lubrication performance of WSB is improved by optimizing the geometric parameters of the lining's surface layer, flume, or designing surface texture, to reduce shafting vibration indirectly. Liu et al. [13] designed micro-hole arrays on the lining and studied the influence of texture on lubrication and vibration damping performance through simulation and experiment. About damping design, Jin et al. [14] designed the bearing bushing as inner bushing and outer bushing, between which there were filled with rubber. The test shows that the structure is provided with a certain damping effect.

In general, the modification methods of bearing material place emphasis on improving tribological properties, in this way, which dilutes the effect of vibration reduction. There is a problem with changing the lining structure, large deformation arising in the soft lining layer under the action of heavy load and offset load, and the structures, such as micro-grooves and textures, will be compacted and lose the damping effect. The essential reason for this problem lies in the coupling between load carrying and vibration reduction in WSB. It is necessary to decouple them. Squeeze film dampers (SFDs) are often employed to provide additional damping and support to lead to a cut of rotor response and forces transmitted to the ground [15, 16]. The Integral Squeeze Film Damper (ISFD) is manufactured through electrical discharge machining (EDM) [17]. In general, the elastic support shape has been removed from C shape, L shape, material removal S shape [18], and material reserved S shape, where the material S reserved shape is the most popular shape at present [19]. ISFD has been successfully applied to the bearings of the steam turbine set [20], gear system [21], supercritical CO<sub>2</sub> expander [22]. Ferrecki P. et al. In 2019, Ertas [23] researched a gas-film lubricated bearing concept with ISFD, and the transient fluid–structure interaction (FSI) simulation work is innovative. Stiffness of the ISFD design is defined by the “S” shape springs, and it absorbs energy through the oil piston/dashpot effect from the “S” structure's gap. The design of separating stiffness from damping can decouple the load carrying and damping functions. For want

of effective vibration reduction, this paper innovatively proposes to introduce ISFD into WSB.

In the present study, the problem in the vibration reduction design of WSB is analyzed, the decoupling design idea of load carrying and vibration reduction is proposed. And the ISFD technology is introduced into the conventional water-lubricated stern bearing (CWSB) to achieve a water-lubricated damper stern bearing (WDSB). The finite element method (FEM) is used to calculate the harmonic response of these two bearings, and the damping structure parameters are optimized. The dynamic characteristics of two bearings are measured on a bearing test rig to verify the vibration reduction effect of WDSB.

## 2 Method of vibration reduction for water-lubricated stern bearing

### 2.1 The coupling problem of load carrying and vibration reduction

A CWSB consists of a liner and a bushing, where the lining is made of polymer composite materials such as nitrile rubber (NBR). Figure 1 presents three kinds of structure schemes. Among them, the design using rubber to carry the load and reduce vibration at the same time remains defective. The dynamic model of CWSB is shown in Fig. 2a, where  $m$  is the vibration mass,  $k$  and  $c$  are the stiffness and damping coefficients of the bearing, respectively, which are formed by the lining and the water film. Under the excitation force  $F$ , the shaft will give response  $x$ . Under the heavy load, an obvious deformation of rubber layer in lining will come up, and the damping effect of rubber will be significantly reduced after a serious extrusion.

From the perspective of vibration isolation, the lining plays a role in vibration isolation. It is hoped that the vibration energy transmitted from the shaft to the bearing block will be minimized. According to the linear vibration isolation theory, the system is provided with a vibration isolation

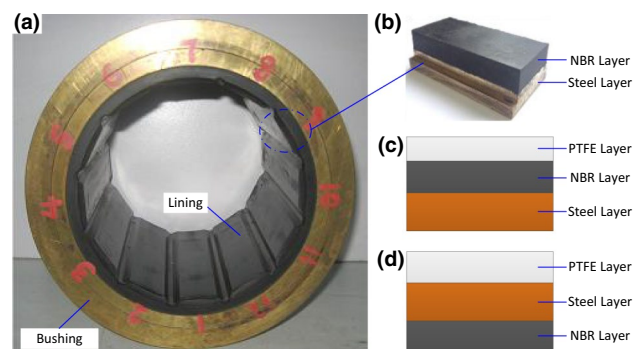


Fig. 1 Three structural schemes of WSB

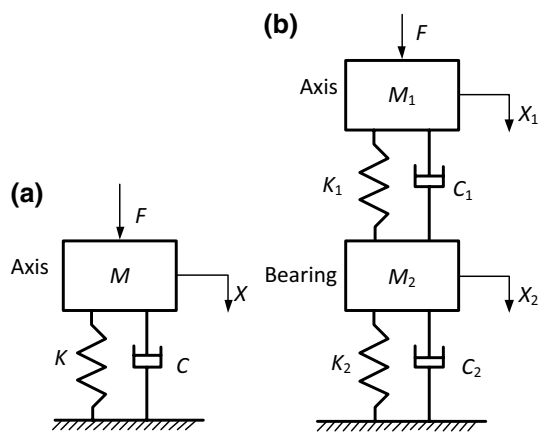


Fig. 2 Dynamic model: a CWSB; b WDSB

effect only when the excitation frequency is greater than  $\sqrt{2}$  times the natural frequency of the system. Therefore, in the case of constant excitation frequency, it is always desirable to minimize the natural frequency of lining. However, in order to improve the carrying capacity, it is required that the bearing has a relatively large stiffness, but high stiffness will inevitably lead to a higher natural frequency. Therefore, the contradiction between high carrying capacity and low natural frequency has become one of the bottlenecks in the development of damping technology of WSB.

### 2.2 Independent design method of load carrying and vibration reduction

In order to solve the contradiction, it is necessary to decouple functions of load carrying and vibration reduction. As shown in Fig. 2b,  $k_1$  and  $c_1$  are the stiffness and damping coefficients composed of the lining and the water film, respectively,  $m_2$  is the bearing mass. Add a damping structure attachment to the back of the CWSB to form a WDSB. The stiffness and damping coefficients of the attachment are  $k_2$  and  $c_2$ , respectively. In order to ensure the high load-carrying capacity of the bearing,  $k_2$  is relatively large. The main features of this design are as follows:

1) Original bearing and attachment are independent. The original lining structure and material are unchanged. By adding an attachment structure to the bearing bushing or on the outer wall of the bearing, the vibration is isolated without damping the carrying capacity.

2) The substructures that implement the functions of load carrying and vibration reduction are independent. That is, the attachment structure has a high stiffness  $k_2$  to achieve high load carrying capacity, and a special substructure provides a large damping  $c_2$  to achieve energy dissipation.

The vibration differential equation of WDSB is:

$$\begin{cases} m_1\ddot{x}_1 + c_1\dot{x}_1 - c_1\dot{x}_2 + k_1x_1 - k_1x_2 = F(t) \\ m_2\ddot{x}_2 - c_1\dot{x}_1 + (c_1 + c_2)\dot{x}_2 - k_1x_1 + (k_1 + k_2)x_2 = 0 \end{cases} \quad (1)$$

By constructing the matrix equation, the response of the journal can be obtained as:

$$X_1(\omega) = F_0 \sqrt{\frac{a^2 + b^2}{g^2 + h^2}} \quad (2)$$

where  $a = k_1 + k_2 - m_2\omega^2$ ,  $b = (c_1 + c_2)\omega$ ,  $g = (k_1 - m_1\omega^2)(k_2 - m_2\omega^2) - (k_1m_1 + c_1c_2)\omega^2$ ,  $h = [(k_1 - m_1\omega^2)c_2 - (k_2 - m_2\omega^2 - m_1\omega^2)c_1]\omega^2$ .

When the structure and working conditions are known, the mass, stiffness, and damping coefficient in the above equation are determined. Supposing  $m_1 = 1100$  kg,  $m_2 = 30$  kg,  $\omega = 20$  Hz,  $F_0 = 3$  kN,  $k_1 = 1 \times 10^7$  N/m,  $k_2 = 1 \times 10^9$  N/m,  $c_1 = 0.4 \times 10^5$  N/(m/s), bring into equations to calculate the journal response with  $c_2$ . WDSB's journal response increases along with the increase in  $c_2$  following a decrease. When  $c_2$  is  $8.1 \times 10^6$  N·s/m, WDSB's journal response is the smallest, about 27.7% lower than that of CWSB.

### 3 The structure scheme of WDSB

In view of the independent design of load carrying and vibration reduction, a WDSB with ISFD (as shown in Fig. 3) is designed. "S" shape gaps are set in the CWSB's bushing. According to the carrying characteristics of WSB, the bearing's attitude angle is very small, about  $5^\circ \sim 20^\circ$ , and the carrying area is concentrated in the range of  $20^\circ \sim 30^\circ$  at the bottom of the bearing [13]. Therefore, the scheme only has two "S"-shaped elastic structures at the bottom of the bearing, which are arranged along the circumference and symmetrical along the vertical centerline.

In order to analyze the effects of the structure on the damping effect, three structural parameters are defined namely oil film clearance  $\delta$ , inner flange height  $s$ , distribution angle  $\theta$  of "S" shape springs, as shown in Fig. 3. The "S" shape springs divide the bushing into two parts, inner flange and outer flange. Oil is enclosed in the "S" shape gaps by end caps, and an oil chamber is arranged on the end cover to store oil. When the bearing is operating, the "S" shape springs will come a rhythmic stretching deformation under the action of the excitation force. The oil is sucked and discharged along the axial direction in the "S" shape gaps, leading to a squeeze effect. At the same time, the "S" spring side wall and the oil cover are relatively running, and a piston/dash-pot effect is formed in the gap between them. They provide energy consumption for vibration reduction.

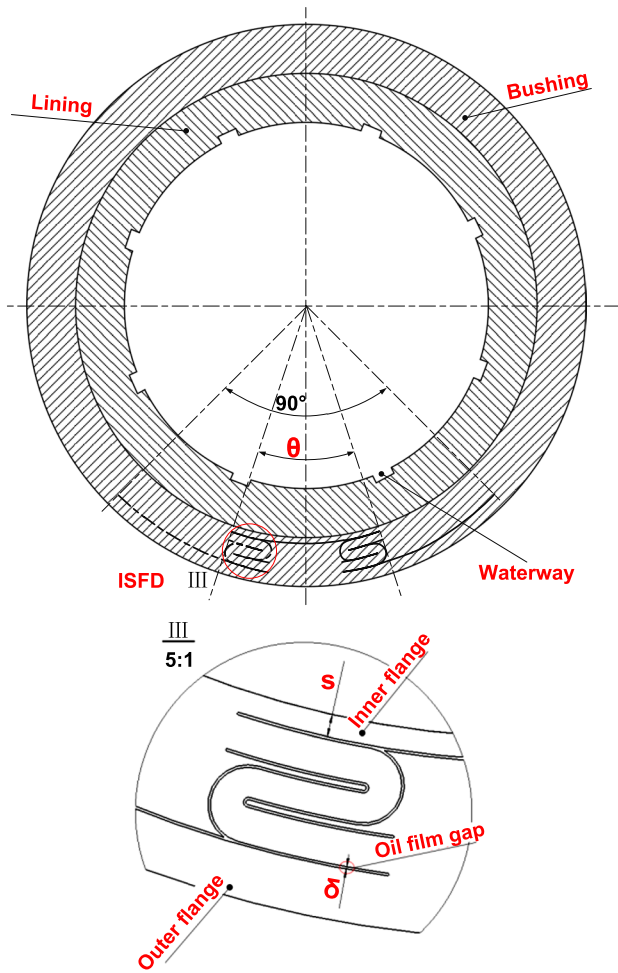


Fig. 3 Structure diagram of the WDSB

The basic structure and physical parameters of the bearing are shown in Table 1.

### 4 Harmonic response analysis of WSB

The natural frequency of the bearing itself is one of the key factors affecting the amplitude of the bearing response when bearing is excited. Firstly, three-dimensional models of two bearings are established, and then the finite element models

are formed in ANSYS software. The contact between the lining and hushing of the bearing is defined as “Bonded.” After the mesh independence test of the model, the CWSB generates 165145 mesh elements and 460,470 mesh nodes. For the WDSB, the mesh at the “S” shape gaps is encrypted, and a total of 178,145 mesh elements and 612,553 mesh nodes are generated for the bearing. The free mode simulation analysis of WDSB is carried out, and the first four modes are shown in Fig. 4. It can be seen that the deformation of WDSB is mainly distributed in lining and bushing near the “S” shape structure, because the stiffness of the “S” shape structure is lower than that of the nearby structure. Moreover, the vibration modes of the first four modes are basically the same, but the positions and angles of the maximum deformation are different.

In order to obtain the response characteristics of WDSB under excitation, the harmonic response analysis using the software ANSYS Workbench is carried out. Based on the calculation results, the maximum response and its frequency are found, which provides a reference for optimizing the structure of WDSB. Due to fast solution speed, considering of damping factor, smooth harmonic response curve and high calculation accuracy, the mode superposition method is chosen. The excitation force  $F(t) = F_0 \sin(\omega t)$ . Where,  $F_0$  is 0.2 MPa, the direction of the excitation force is vertically downward, loaded on the lower surface of lining. According to the modal analysis, the natural frequency of WDSB constrained mode is in the range of 2500 ~ 5500 Hz. Therefore, the scanning frequency is set to 2500 ~ 5500 Hz. As shown in Fig. 4, the mode shape is mainly concentrated on the “S” shape structure and the lining above it. Therefore, the part under the lining is extracted for analysis, as shown in Figs. 5 and 6.

As  $\delta$  increases, the response frequency decreases first and then increases. The frequency at the maximum displacement response (FMDR) and the frequency at the maximum stress response (FMSR) are substantially coincident at the same clearance. With the rise in  $\delta$ , the maximum displacement response (MDR) tails off. WDSB with  $\delta$  of 0.2 mm is compared with CWSB, as shown in Fig. 7. The displacement response peak value of WDSB is remarkably smaller than that of CWSB, but WDSB has more response peaks. The MDR of CWSB is 1.31 mm, and the MDR of WDSB is

Table 1 Basic parameters of the water-lubricated stern bearing

Parameter	Value	Parameter	Value
Inner diameter of bearing/mm	150	Young’s modulus of lining/MPa	490
Outer diameter of bearing/mm	230	Density of lining/(kg/m <sup>3</sup> )	1510
Bearing length/mm	150	Poisson ratio of lining	0.45
Thickness of lining/mm	20	Young’s modulus of bushing/MPa	$2.11 \times 10^5$
Flume number	8	Density of bushing/(kg/m <sup>3</sup> )	7 850
Flume depth/mm	6	Poisson ratio of bushing	0.28



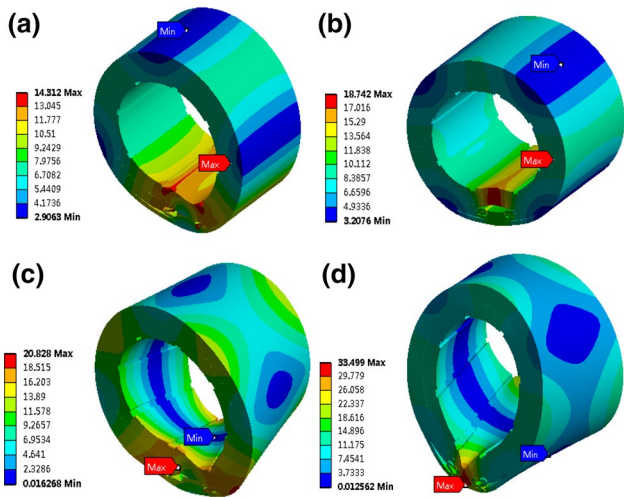


Fig. 4 Free mode of bearing: a First mode; b Second mode; c Third mode; d Fourth mode

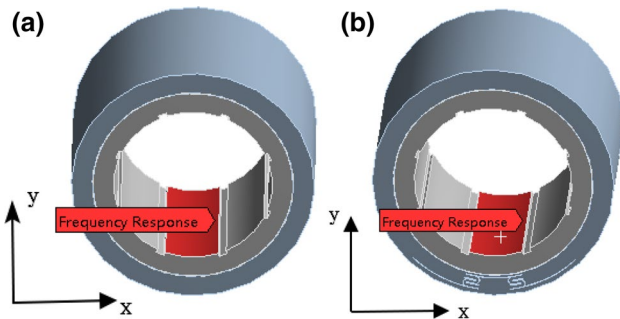


Fig. 5 Extract location: a CWSB; b WDSB

0.42 mm when  $\delta$  is 0.25 mm, which presents a drop of 67.9% around, indicating that WDSB leads to a dramatic vibration cut.

Both CWSB and WDSB with  $\delta$  of 0.15 mm show only one stress response peak, while WDSBs with  $\delta$  of 0.2 mm and 0.25 mm have multiple stress response peaks. The maximum stress response (MSR) increases first and then decreases with the increase in  $\delta$ . The MSR of CWSB is the smallest, which is 36.9 MPa. When  $\delta$  is 0.25 mm, the MSR is 42.2 MPa, which increases by about 12.6% compared with CWSB, of which reason is “S” shape structure reduces bearing’s stiffness and increases stress under the excitation.

The oil film clearance  $\delta$  is 0.2 mm, and the distribution angle  $\theta$  is 10°. After changing the inner flange height  $s$ , calculation results are shown in Fig. 8. As  $s$  increases, the MDR increases first and then decreases. When  $s$  is 2.5 mm, the MDR is the smallest at 0.49 mm. When  $s$  is 4 mm, the MDR is the largest at 0.72 mm. As  $s$  increases, the MSR drops at the heel of slides. When  $s$  is 3.5 mm, the MSR is the largest at 65.2 MPa, and when 2.5 mm, the MSR is the

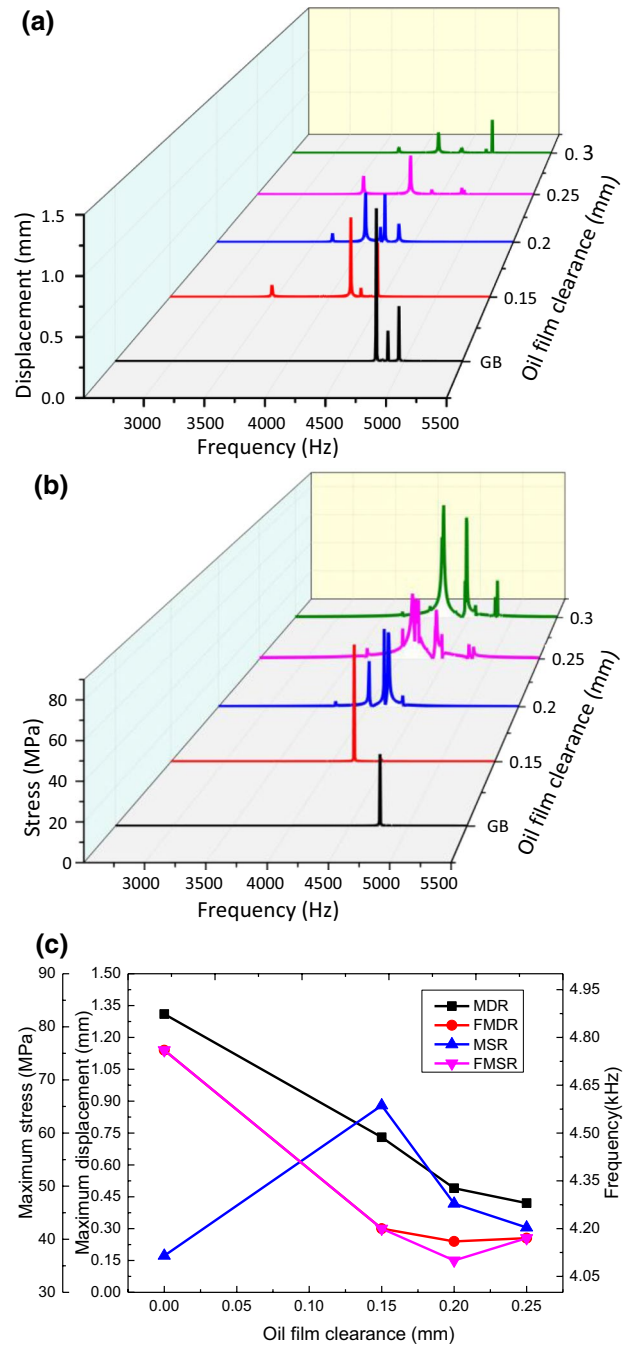
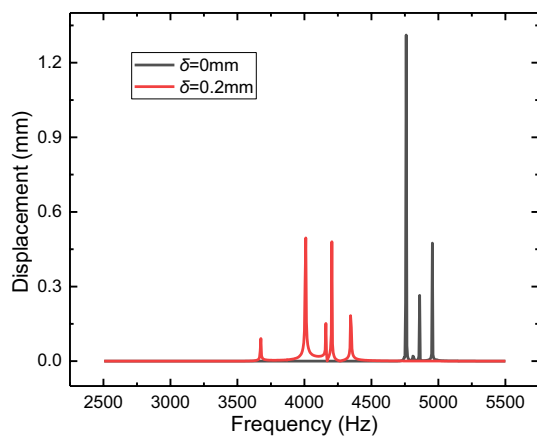


Fig. 6 Distribution of harmonic response under different oil film clearance: a Frequency-displacement response; b Frequency-stress response; c Maximum value

smallest, 46.7 MPa. In summary, when  $s$  is 2.5 mm, the “S” shape structure brings about the most striking reduction in the displacement response and the minimum stress response.

When the oil film clearance  $\delta$  is 0.2 mm and the inner flange height  $s$  is 2.5 mm. The calculation results are shown in Fig. 9 under different distribution angle  $\theta$ . With the increase in  $\theta$ , the MDR decreases first and then increases.



**Fig. 7** Displacement responses between CWSB and WDSB with an oil film clearance of 0.2 mm

When  $\theta$  is taken as  $10^\circ$  and  $11^\circ$ , respectively, MDRs are close. When  $\theta$  is  $8^\circ$ , the MDR is the largest at 1.15 mm, and when  $11^\circ$ , the MDR is the smallest, 0.48 mm. The MSR with  $\theta$ , in the same way, climbs in the wake of a drop, and the minimum MSR appears at  $\theta$  of  $11^\circ$ . When  $\theta$  is  $8^\circ$ , the MSR is the largest, 86.9 MPa, and when  $11^\circ$ , the MSR achieves the smallest at 42.3 MPa. In summary, when  $\theta$  is  $11^\circ$ , the “S” shape structure performs the best damping effect.

Three parameters of “S” shape structure can influence the vibration and stress in a coupled manner. The oil film clearance and distribution angle have similar effects. And the effect of the inner flange height on the vibration is opposite to the above two parameters.

## 5 Test

### 5.1 Test rig

The vibration reduction effect verification of WDSB is conducted on a test rig, as shown in Fig. 10. The motor power of the drive module is 15 kW, and the maximum rotational speed is 1200r/min. The shaft is supported by two rolling bearings, and the test bearing is suspended on the shaft. The journal at the test bearing has a ZQSn10-2 bushing with a length of 175 mm and an outer diameter of  $\varnothing 150$  mm. The loading module adopts hydraulic loading mode, the force acts on the bottom of the test bearing, and the maximum load is 1.5t.

### 5.2 Test Bearing

The basic parameters of CWSB and WDSB are the same (as shown in Table 1), except that WDSB has a damping structure on its bushing. According to the simulation results, the

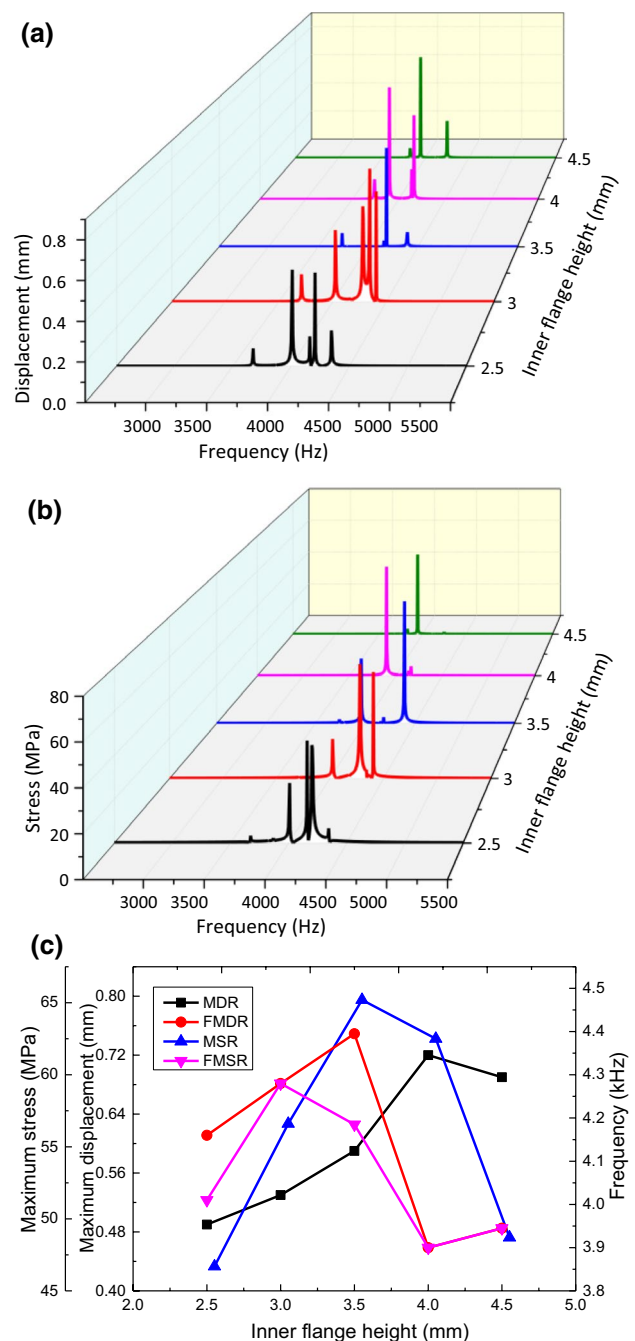


**Fig. 8** Distribution of harmonic response under different inner flange heights: **a** Frequency-displacement response; **b** Frequency-stress response; **c** Maximum value

parameters of damping structure are selected as follows:  $\delta$  is 0.2 mm,  $s$  is 2.5 mm, and  $\theta$  is  $11^\circ$ . The “S” shape structure is machined by wire-cutting technology, and the “S” shape gap is filled with lubricating oil with a density of  $870 \text{ kg}\cdot\text{m}^{-3}$  and a viscosity of  $0.048 \text{ Pa}\cdot\text{s}$ . Milling grooves on both sides of the “S” shape structure, the groove can store oil, by installing a sealing cover on the groove, and machining a

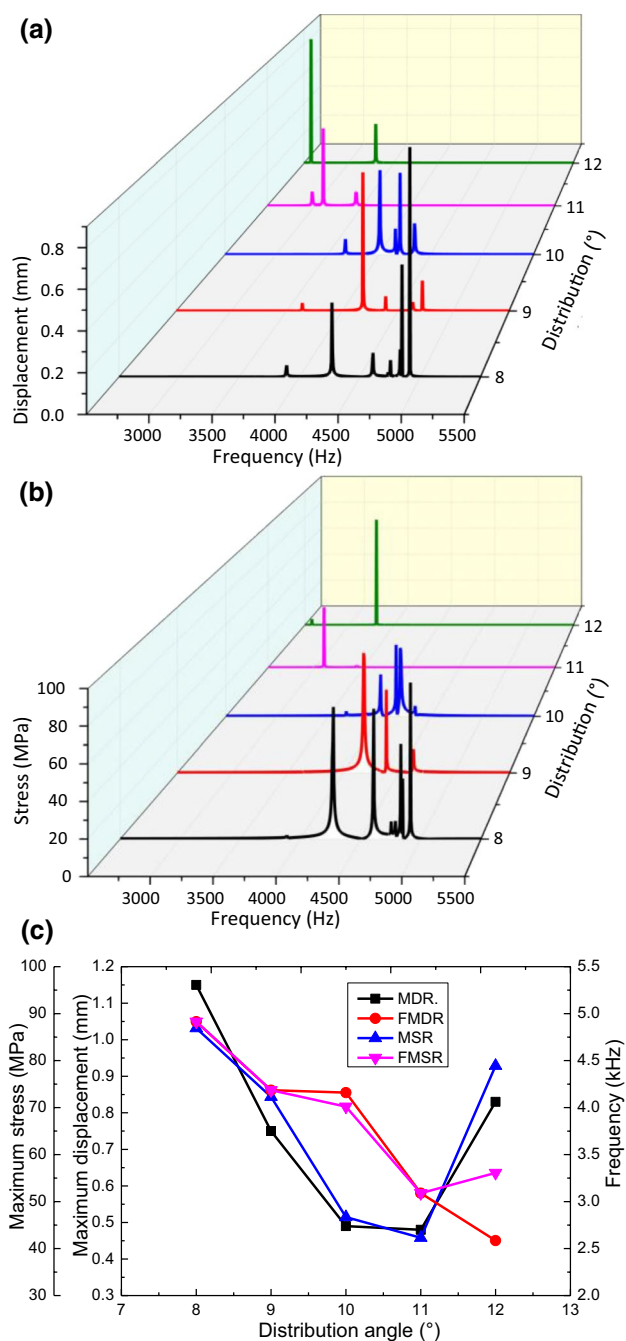


**Fig. 9** Distribution of harmonic response under different distribution angles: **a** Frequency-displacement response; **b** Frequency-stress response; **c** Maximum value

ring groove on the inside of the sealing cover, and a rubber seal is installed in the ring groove to avoid leakage of oil. Two test bearings are shown in Figs. 11 and 12.

### 5.3 The test scheme and procedure

The test scheme is as follows: The friction torque of the rotating component is measured by a torque meter. Removing the

friction torque of supporting bearings and seals, and friction torque, the friction coefficient of test bearing can be obtained. Besides, the torque meter can also give a rotational speed signal. A force sensor is installed between loading rod and test bearing to obtain force signal, and the ratio of loading force to bearing's projected area is the specific pressure. Two accelerometers (Type 4514B, Brüel & Kjær Sound and Vibration Measurement A/S, Denmark. Sensitivity is 9.5 mv/g. Range is 1 Hz to 10 kHz) are installed on top of the test bearing to measure the horizontal and vertical vibration. The measurement module is an acoustic and vibration measuring instrument (Type 3053-B-120, Brüel & Kjær Sound and Vibration Measurement A/S, Denmark), and the frequency domain data can be obtained by Fourier transform from the time domain signal. The analysis bandwidth is 25.6 kHz, and the frequency resolution is 25,600/6400.

The bearing static stiffness measure principle is shown in Fig. 13, and two dial indicators are symmetrically mounted on both ends of test bearing. When the speed is 0 r/min, the loading device applies an upward force to test bearing, the force sensor measures loading force, and the dial indicators measure upward displacement of bearing. The test values of two dial indicators are averaged to obtain the deformation of bearing lining. After deducting bearing's weight, the load force is load, and the ratio of load to deformation is bearing's static stiffness. The specific pressure is in the range of 0~0.4 MPa.

Three kinds of load: 0.2, 0.3, 0.4 MPa. Five kinds of speeds: 80, 100, 150, 200, 300 r/min. The lubrication water flow is 22 L/min, and the water temperature is 18 °C.

## 5.4 Experimental results and discussion

### 5.4.1 Static stiffness test

The static stiffness test was carried out on two bearings, respectively, by using the above principle. Under the same test condition, each bearing was measured repeatedly for 5 times, and then the results were averaged, which is the test value of static stiffness. The test results are shown in Table 2. It can be seen that WDSB's deformation is larger under the same load and its stiffness is reduced by about 26.1% compared with CWSB. In addition, the simulated value of CWSB's static stiffness is 11.2% relative to its experimental value, and the simulated value by FEM of WDSB's static stiffness is 10.6% relative to its experimental value, which verifies the simulation results are reliable.

### 5.4.2 The effects of rotational speed on vibration

Firstly, the no-load test is performed to measure bearing vibration at different speed. Taking them as the initial value, the effects of working conditions on bearing vibration is



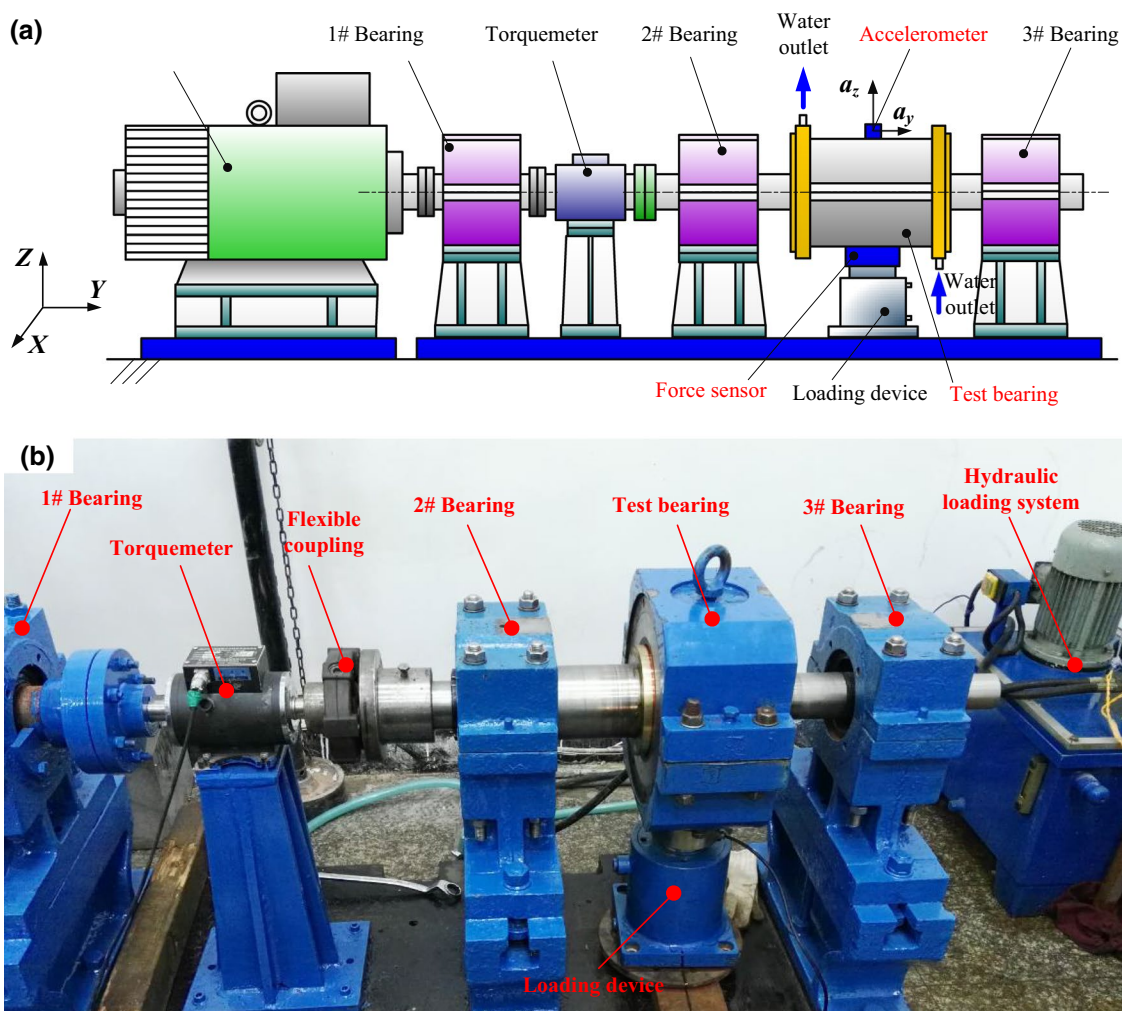


Fig. 10 Test rig: a Composition; b Photograph



Fig. 11 Photograph of a CWSB

analyzed. In the no-load test, the maximum vibration amplitude of test bearing in horizontal direction under different rotating speeds is less than  $15 \text{ mm/s}^2$ , and the one in vertical direction is below  $50 \text{ mm/s}^2$ .

The load of test bearing is  $0.4 \text{ MPa}$ , and the rotational speed is  $80 \text{ r/min}$ ,  $100 \text{ r/min}$ ,  $150 \text{ r/min}$ ,  $200 \text{ r/min}$  and  $300 \text{ r/min}$ , respectively. The frequency-domain of vibration acceleration of two bearings in vertical and horizontal directions under different speeds is shown in Fig. 14. It can be seen that the vibration amplitude of two bearings in horizontal direction is smaller than that in vertical direction, and horizontal vibration has more peaks than vertical direction. The vibration peaks in vertical direction are mainly concentrated within  $1000 \text{ Hz}$ , and the vibration amplitudes in vertical direction are mainly distributed in two frequency ranges of  $0 \text{ Hz}$  to  $1000 \text{ Hz}$  and  $4000 \text{ Hz}$  to  $5000 \text{ Hz}$ . In addition, the rotation rate increases and vibration amplitudes of both directions get dragged along for the ride. Comparing vibration amplitudes between two bearings, it can be seen that



Fig. 12 Photograph of a WDSB

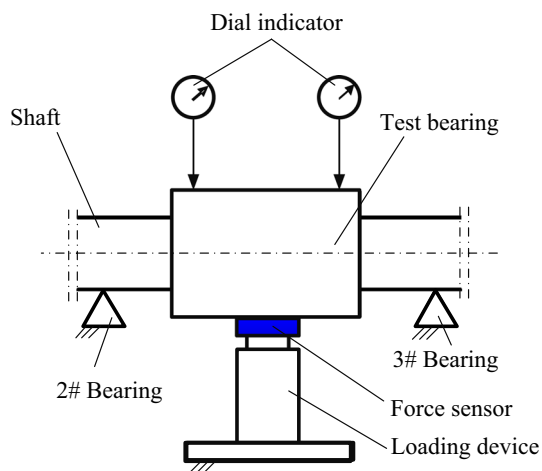


Fig. 13 Measure principle of bearing’s static stiffness

WDSB’s vibration amplitude is significantly smaller than that of CWSB under the same working conditions in both directions, indicating that WDSB is provided with a better damping effect.

In order to quantitatively illustrate the damping effect, the maximum value (MAX) and the Root Mean Square

(RMS) value of vibration amplitude in horizontal direction under different speeds are shown in Fig. 15. The RMS of a spectrum considering window correction factors (Hanning window) can be expressed as follows:

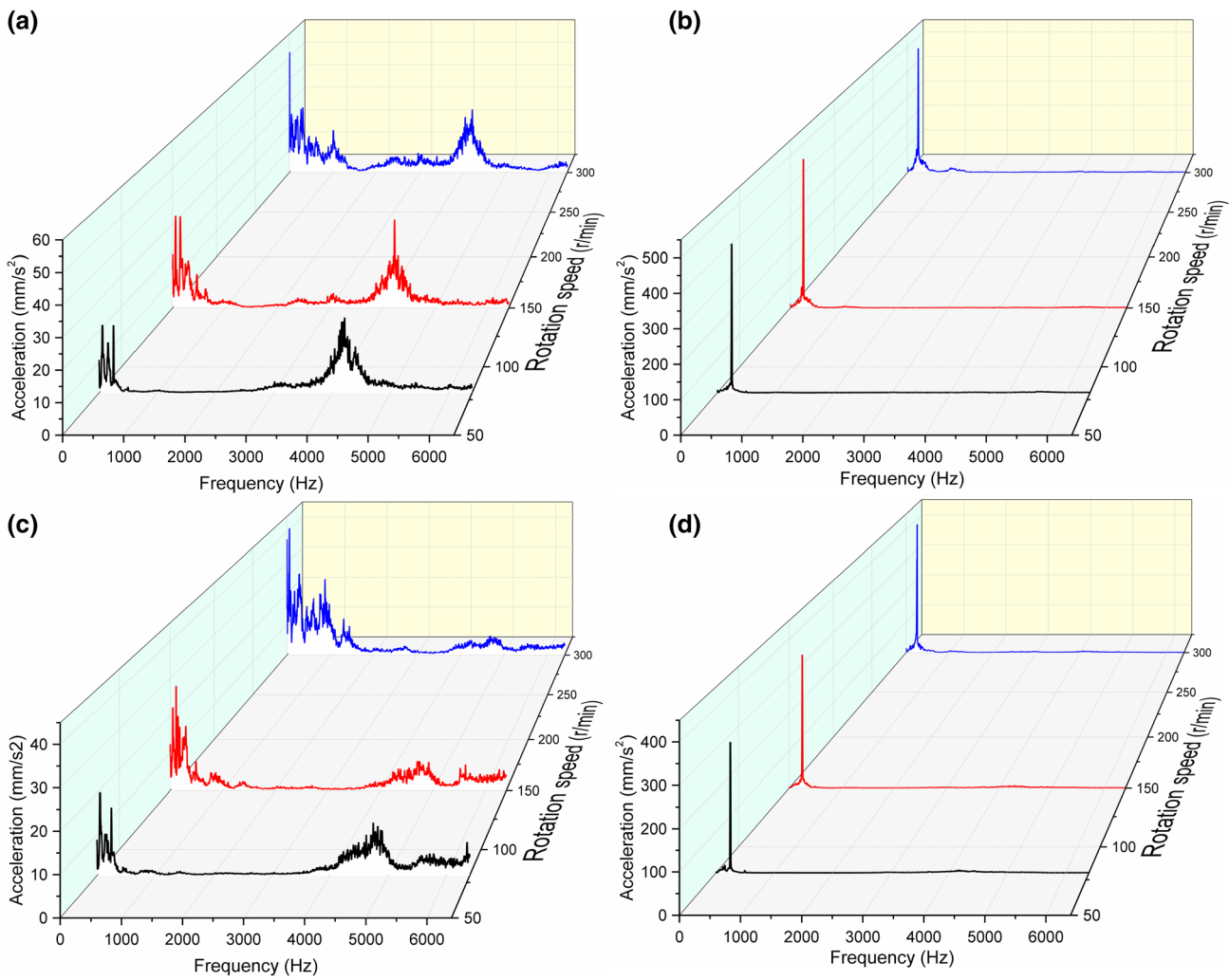
$$RMS = \frac{1.63}{2} \sqrt{\frac{A_0^2}{2} + \sum_{i=1}^{k-1} A_i^2 + \frac{A_k^2}{2}} \tag{3}$$

where  $A$  represents the amplitude of a spectral line.  $A_0$  is the first spectral line, and  $A_k$  is the last spectral line. The overall level is from 0 ~ 6400 Hz.

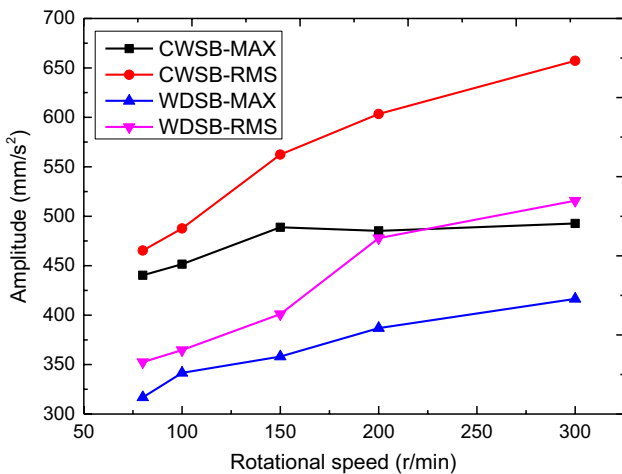
It can be seen that at low speed, as the rotation rate goes up, MAX value and RMS value of two bearings increase. But when the rotational speed is 200 r/min, MAX value of CWSB is smaller than that in 150 r/min. As the rotational speed increases, the gap between two bearings’ MAX tends to decrease, but the gap between two bearings’ RMS remains overall unchanged. RMS has an average connotation, so it is more universal to use it to explain the damping effect. It shows that the damping effect of WDSB has the ability of keeping when the speed changes. When rotational speed is 300 r/min, compared with CWSB, WDSB’s MAX amplitude in horizontal direction is reduced by about 76.3 mm/s<sup>2</sup>,

Table 2 Simulation and experimental results of deformation and static stiffness of two bearings

Types	Simulation value of deformation/mm	Experimental value of deformation/mm	Relative difference/%	Simulation value of static stiffness/ $\times 10^7$ (N/m)	Experimental value of static stiffness/ $\times 10^7$ (N/m)	Relative difference/%
CWSB	0.302	0.336	10.1	2.98	2.68	11.2
WDSB	0.410	0.454	9.7	2.19	1.98	10.6



**Fig. 14** Frequency domain diagrams of acceleration of two bearings under different speeds: **a** CWSB- Horizontal direction; **b** CWSB- Vertical direction; **c** WDSB- Horizontal direction; **d** WDSB- Vertical direction



**Fig. 15** MAX and RMS of two bearings in horizontal direction under different rotational speeds

accounting for about 15.5% of that of CWSB. WDSB’s RMS amplitude is reduced by about 141.5 mm/s<sup>2</sup>, accounting for about 21.5% of that of CWSB.

**5.4.3 The effects of load on vibration**

The rotational speed is 200r/min, and the load is 0.2 MPa, 0.3 MPa and 0.4 MPa, respectively. The vibration acceleration spectrum of two bearings in horizontal direction under different loads is shown in Fig. 16. It can be seen that under different loads, both bearings have large vibration amplitudes in two frequency ranges of 0~350 Hz and 3800~5100 Hz. From the local enlarging graph, about three distinct vibration peaks appear for both bearings in the previous frequency range. When it is less than 700 Hz, the vibration amplitude of two bearings performs a great consistency, that is, the frequency corresponding to the vibration peak is close. When the frequency is 700~1700 Hz, WDSB has two

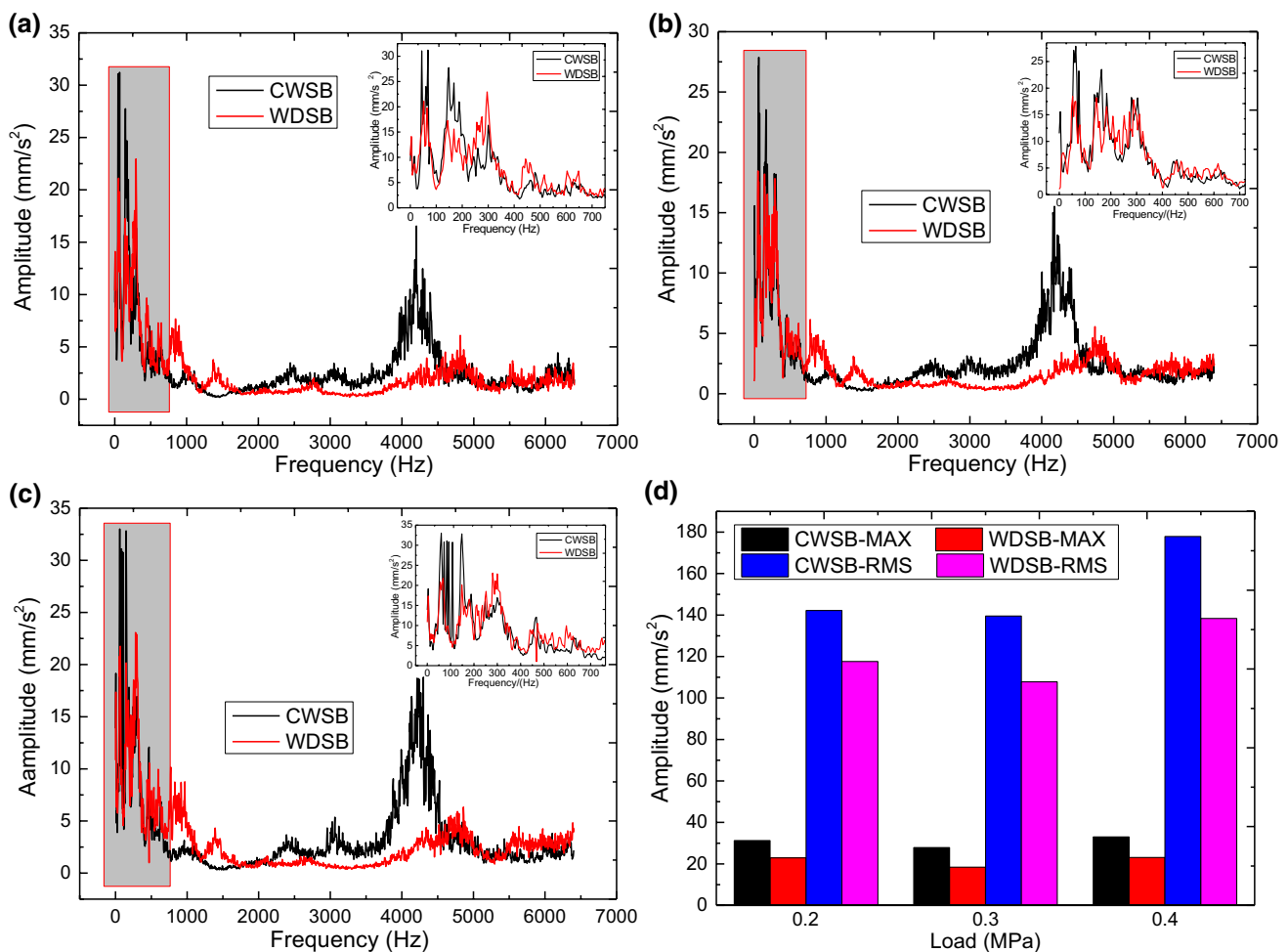


**Fig. 16** Frequency domain of vibration acceleration of two bearings in horizontal direction under different loads: **a** 0.2 MPa; **b** 0.3 MPa; **c** 0.4 MPa; **d** MAX and RMS

vibration peaks, but CWSB has only one. The corresponding frequency of vibration peaks of two bearings is quite different, and the vibration peak of WDSB is larger than that of CWSB. When it is greater than 700 Hz, the vibration peak of WDSB is smaller than that of CWSB, and the corresponding frequency of WDSB is also significantly larger than that of CWSB. MAX and RMS of two bearings' vibration amplitude are shown in Fig. 16 (d). It can be seen that the maximum amplitude of WDSB is significantly smaller than that of CWSB, the reduction is about 10 mm/s<sup>2</sup>, and the relative reduction is 30.3% to 32.0%. A rise in the gap between two bearings' RMS comes as the load continues to increase, the reduction is 24.6 mm/s<sup>2</sup> and 39.6 mm/s<sup>2</sup>, respectively, when the load is 0.2 MPa and 0.4 MPa, and the relative reduction is 27.3% and 22.2%, respectively (Fig. 16).

The vibration acceleration spectrum of two bearings in vertical direction under different loads is shown in Fig. 17. It can be seen that both bearings only occur two vibration

wave peaks, and the same corresponding frequency of the peaks is observed in two bearings, 248 ~ 1050 Hz, respectively, where the first peak is much larger than the second one. According to the first vibration peak, a local enlarging graph is given. It can be seen that as load increases, the maximum vibration of two bearings comes to increase. When the load is 0.2 MPa, CWSB's amplitude is 195.3 mm/s<sup>2</sup>, but that of WDSB is 55.0 mm/s<sup>2</sup>, and the relative reduction is 71.8%. When the load is 0.3 MPa and 0.4 MPa, the relative reduction is 40.5% and 20.3%, respectively, that is, as load increases, the relative reduction gradually decreases. RMS amplitudes of two bearings under three loads are shown in Fig. 17d. It can be seen that load increases, so do RMS of two bearings. When the loads are 0.2 MPa, 0.3 MPa and 0.4 MPa, the relative reduction in RMS are 47.8%, 36.2% and 20.8%, respectively, that is, the relative reduction in RMS also decreases with a rise in load.

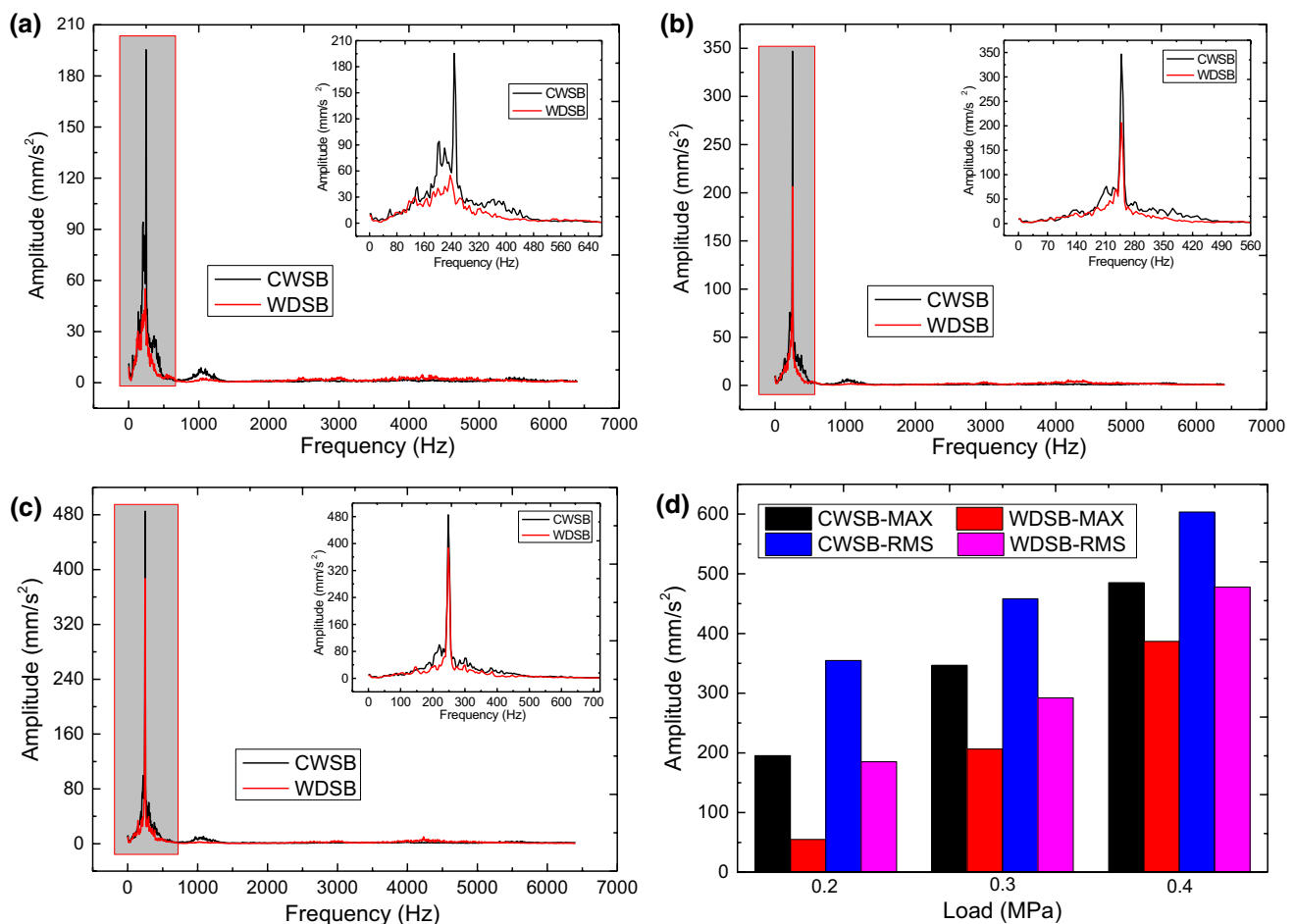


**Fig. 17** Frequency domain of vibration acceleration of two bearings in vertical direction under different loads: **a** 0.2 MPa; **b** 0.3 MPa; **c** 0.4 MPa; **d** MAX and RMS

## 6 Conclusions

As for the particular investigated bearing, some far-reaching conclusions have been drawn.

(1) CWSB has a contradiction between high carrying capacity and low natural frequency, which can be resolved by the independent design of load varying and vibration reduction. According to the simulation results of harmonic response, the maximum displacement response decreases along with an increase in oil film clearance. The maximum displacement response of CWSB is 1.31 mm, and the maximum displacement response of WDSB is 0.42 mm when the oil film clearance is 0.25 mm, which is reduced by about 67.9%.

(2) When the load is 0.4 MPa, vibration amplitudes of WDSB are significantly smaller than those of CWSB under various speeds. As the rotation rate speeds, the gap between two bearings' RMS remains overall unchanged. It shows that the damping effect of WDSB has the ability of keeping when the speed changes.

(3) When rotational speed is 200r/min, both the vibration maximum amplitude and RMS of two bearings increase accompanied by an increase in load. When the load is 0.2 MPa, compared with CWSB, the maximum amplitude of WDSB in vertical direction is reduced by about 71.8%, and by about 47.8% for the relative reduction in RMS, which verifies the damping effect of WDSB is remarkable.

Future works will focus mainly on the influence of the clearance oil's viscosity on the damping performance and the coupling effect between the lining and the ISFD.

**Acknowledgments** This paper is supported by the National Defense Pre-Research Foundation of China (No. 61402100402).



## Appendix

Acronyms	Full name
CWSB	Conventional water-lubricated stern bearing
WDSB	Water-lubricated damping stern bearing
MDR	Maximum displacement response
RMS	Root mean square
WSB	Water-lubricated stern bearing
SFDs	Squeeze film dampers
ISFD	Integral squeeze film damper
EDM	Electrical discharge machining
FSI	Fluid–structure interaction
NBR	Nitrile rubber
FMDR	Frequency at the maximum displacement response
FMSR	Frequency at the maximum stress response
MSR	Maximum stress response
FEM	Finite element method
MAX	Maximum value

## References

- Chen F, Chen Y, Hua HX (2019) Vibration analysis of a submarine elastic propeller-shaft-hull system using FRF-based substructuring method. *J Sound Vib* 443:460–482. <https://doi.org/10.1016/j.jsv.2018.11.053>
- Xie XL, Qin H, Xu YL et al (2019) Lateral vibration transmission suppression of a shaft-hull system with active stern support. *Ocean Eng* 172:501–510. <https://doi.org/10.1016/j.oceaneng.2018.12.004>
- Simpson TA, Ibrahim RA (1996) Nonlinear friction-induced vibration in water-lubricated bearings. *J Vib Contr* 2:87–113. <https://doi.org/10.1177/107754639600200106>
- Das S, Guha SK (2019) Numerical analysis of steady-state performance of misaligned journal bearings with turbulent effect. *J Braz Soc Mech Sci* 41:81. <https://doi.org/10.1007/s40430-019-1583-4>
- Jadhav S, Thakre GD, Sharma SC (2018) Numerical modeling of elastohydrodynamic lubrication of line contact lubricated with micropolar fluid. *J Braz Soc Mech Sci* 40:326. <https://doi.org/10.1007/s40430-018-1249-7>
- Ouyang W, Zhang XB, Jin Y et al (2018) Experimental study on the dynamic performance of water-lubricated rubber bearings with local contact. *Shock Vib* 2018:1–10. <https://doi.org/10.1155/2018/6309727>
- Litwin W (2016) Influence of local bush Wear on water lubricated sliding bearing load carrying capacity. *Tribol Int* 103:352–358. <https://doi.org/10.1016/j.triboint.2016.06.044>
- Kuang FM, Zhou XC, Huang J et al (2019) Machine-vision-based assessment of frictional vibration in water-lubricated rubber stern bearings. *Wear* 426:760–769. <https://doi.org/10.1016/j.wear.2019.01.087>
- Zhang ZG, Zhang ZY, Huang XC et al (2014) Stability and transient dynamics of a propeller–shaft system as induced by nonlinear friction acting on bearing-shaft contact interface. *J Sound Vib* 333:2608–2630. <https://doi.org/10.1016/j.jsv.2014.01.026>
- Yan ZM, Zhou XC, Qin HL et al (2015) Study on tribological and vibration performance of a new UHMWPE/graphite/NBR water lubricated bearing material. *Wear* 333:872–878. <https://doi.org/10.1016/j.wear.2014.12.054>
- Orndorff RL (2000) New UHMWPE/rubber bearing alloy. *J Tribol-Trans ASME* 122:367–373. <https://doi.org/10.1115/1.555361>
- Litwin W (2015) Properties comparison of rubber and three layer PTFE-NBR-bronze water lubricated bearings with lubricating grooves along entire bush circumference based on experimental tests. *Tribol Int* 90:404–411. <https://doi.org/10.1016/j.triboint.2015.03.039>
- Gong JY, Jin Y, Liu ZL et al (2019) Study on influencing factors of lubrication performance of water-lubricated micro-groove bearing. *Tribol Int* 129:390–397. <https://doi.org/10.1016/j.triboint.2018.08.035>
- Huang L, Jin Y, Liu ZL et al (2016) Influence of damping layer on dynamic performance of water-lubricated rubber bearings. *Noise Vib Contr* 36:32–37
- Bouzidane A, Thomas M (2007) Equivalent stiffness and damping investigation of a hydrostatic journal bearing. *Tribol Trans* 50:257–267. <https://doi.org/10.1080/10402000701309745>
- Gehannin J, Arghir M, Bonneau O (2016) A volume of fluid method for air ingestion in squeeze film dampers. *Tribol Trans* 59:208–218. <https://doi.org/10.1080/10402004.2015.1023409>
- Andrés LS, De Santiago O (2004) Imbalance response of a rotor supported on flexure pivot tilting pad journal bearings in series with integral squeeze film dampers. *J Eng Gas Turbines Power-Trans ASME* 126:408–415. <https://doi.org/10.1115/1.1492831>
- De Santiago O, Andrés LS, Oliveras J (1999) Imbalance response of a rotor supported on open-ends integral squeeze film dampers. *J Eng Gas Turbines Power-Trans ASME* 121:718–724. <https://doi.org/10.1115/1.2818532>
- Perfecki P, Zapoměl J, Gebauer M et al (2019) A computational fluid dynamics investigation of the segmented integral squeeze film damper. *MATEC Web of Conferences* 254:1–11. <https://doi.org/10.1051/mateconf/201925408005>
- Ertas B, Cerny V, Kim J et al (2015) Stabilizing a 46 MW multistage utility steam turbine using integral squeeze film bearing support dampers. *J Eng Gas Turbines Power-Trans ASME* 137:052506. <https://doi.org/10.1115/1.4028715>
- Lu KH, He LD, Zhang YP (2017) Experimental study on vibration reduction characteristics of gear shafts based on ISFD installation position. *Shock Vib* 2017:1–10. <https://doi.org/10.1155/2017/7246356>
- Ertas B, Delgado A, Moore J (2018) Dynamic characterization of an integral squeeze film bearing support damper for a supercritical CO<sub>2</sub> expander. *J Eng Gas Turbines Power-Trans ASME* 140:052501. <https://doi.org/10.1115/1.4038121>
- Ertas B (2019) Compliant hybrid gas bearing using integral hermetically sealed squeeze film dampers. *J Eng Gas Turbines Power-Trans ASME* 141:101020. <https://doi.org/10.1115/1.4044644>

**Publisher's Note** Springer Nature remains neutral with regard to jurisdictional claims in published maps and institutional affiliations.